American Mineralogist, Volume 84, pages 138–143, 1999

Computer simulation of pressure-induced structural transitions in MgO [001] tilt grain boundaries

Duncan J. Harris, Graeme W. Watson, and Stephen C. Parker*

School of Chemistry, University of Bath, Bath, BA2 7AY, United Kingdom

Abstract

Atomistic simulations using lattice and molecular dynamics were carried out on the {210}, {310}, and {410} tilt grain boundaries of MgO as a function of pressure up to 100 GPa at a single temperature of 600 K. The calculations show a significant change in the structure of the tilt grain boundaries as pressure increases. The results show that, beyond the previously identified reversible pressure induced collapse of the channel structure, an irreversible shear was identified that forms a mirror grain boundary, which does not possess well-defined dislocation cores and is consequently denser. These mirror boundaries are energetically more favorable than the symmetric boundaries at elevated pressures. As applied pressure approaches 100 GPa a reversible structural transition occurs causing the boundaries to shear perpendicular to the boundary plane forming highly dense structures that contained seven coordinate ions at the boundary and the presence of an edge dislocation-like structure. We suggest that differences between the boundary structures seen in the HREM studies with those predicted by simulations may result from stresses upon the crystal during preparation causing irreversible shearing.

Introduction

One of our ultimate goals is to model the behavior of rocks at elevated pressures and temperatures, which to a great extent depend on the properties of the grain boundaries, such as strength (Kingery 1974) and creep (Poirier 1985). We have begun by considering MgO, which is a simple model material and is believed to be a significant component of the lower mantle (Katsura 1997). The structure of grain boundaries in NiO, isostructural with MgO, was characterized in experimental studies using high-resolution electron microscopy by Merkle and Smith (1987a, 1987b) and Merkle (1994), who proposed a structure for the boundary that was dissimilar to the structures previously suggested by simulations (Duffy and Tasker 1983; Harding et al. 1989).

Computer simulation techniques were used extensively for modeling the effect of pressure on mineral structures, properties, and phase stabilities (Parker 1983; Parker and Price 1989; Matsui and Price 1992; Watson and Parker 1995; Watson et al. 1997). More recently, ab initio methods were used for mineral structure predictions (Brodholt et al. 1996; Darco et al. 1996). However the effect of pressure on grain boundaries has not been simulated, in part because of the many atoms required for ab initio methods. For this reason atomistic simulation methods were used in this work.

In previous work (Harris et al. 1996), we considered the effect of pressure up to 40 GPa upon the symmetric tilt grain boundaries of MgO. The calculations showed that the boundaries underwent a structural transition where the channels forming the boundary collapsed to form a denser structure. This process was found to be reversible upon releasing pressure although a small energy was required to initiate the reversal for the higher index boundaries due to the increase in bond density across the boundary. This paper describes the effect of higher pressures that more closely match those of the lower mantle, focusing on the structures of the {210}, {310}, and {410} tilt grain boundaries of MgO. The previous calculations showed that temperature had little effect upon the boundary properties thus only one temperature, 600 K, is studied.

Methods

Atomistic simulation techniques based on the Born model of solids use interatomic potentials comprising long-range electrostatic and short-range interactions to describe the forces between the ions. The long-range Coulombic interactions converge slowly as a function of increasing ion separation that is overcome using the mathematical transformation of Ewald (1921) is used. The short-range forces were described using a Buckingham potential of the form

$$V(r_{ij}) = A_{ij}\exp\left(\frac{-r_{ij}}{\rho_{ij}}\right) - \frac{C_{ij}}{r_{ij}^6} \quad (1)$$

where A_{ij}, r_{ij}, and C_{ij} are the adjustable parameters and r_{ij} is the inter-ionic separation between ions i and j.

In this work, the potential model of Sangster and Stoneham (1981) was used to model the forces acting

* E-mail: s.c.parker@bath.ac.uk

0003–004X/99/0102–0138$05.00

between the ions. This potential uses valence charges and incorporates the shell model of Dick and Overhauser (1958) to simulate the electronic polarisability of the ions. The potential model was obtained by adjusting the potential parameters until the calculated properties closely matched those measured experimentally. The experimental data included structure, elastic constants, dielectric constants, and the phonon frequencies given in Sangster et al. (1970). The simulation cells containing the three tilt grain boundaries were generated by first considering the two surfaces, i.e., (1) the (210) and $(2\bar{1}0)$, (2) the (310) and $(3\bar{1}0)$, and (3) (410) and $(4\bar{1}0)$ and moving one relative to the other (allowing the ions to fully relax) until the minimum energy grain boundary structure was located. We next generated a simulation cell, which was periodic in three dimensions by including two grain boundaries, pointing in opposing directions where the atom coordinates at the boundary were those found using the earlier energy minimization. Thus the simulation cell contained two boundaries each separated by bulk crystal. We then modeled the boundaries using two methods, namely lattice dynamics (LD) and molecular dynamics (MD).

The LD method that is embodied in the computer code PARAPOCS (Parker and Price 1989; Watson et al. 1997) minimizes the crystal structure with respect to the Gibbs free energy that is given by

$$G = U_{\text{stat}} + U_{\text{vib}} - TS_{\text{vib}} + P_{\text{app}}V \qquad (2)$$

where U_{stat} is the lattice energy, U_{vib} is the vibrational energy contribution including the zero point energy, T is the temperature, S_{vib} is the vibrational entropy, P_{app} is the applied pressure, and V is the volume. The thermal contribution to the free energy was calculated from the normal modes of vibration of the solid by sampling several points in the Brillouin zone using the approach described by Born and Huang (1954); the number of points chosen for sampling depends upon the temperature and the size of the cell. As the cells required for this work were large, 240 atoms for the {210}, 264 for the {310}, and 360 for the {410} boundaries, only one point at (¼,¼,¼) in the Brillouin zone was used although test calculations with eight points gave almost identical results. Thus, to predict structures at high pressure the total pressure, which is defined as the sum of the kinetic, mechanical, and applied pressures, is minimized with respect to volume.

The MD method used the code QCTPMD (Matsui 1989; Watson et al. 1995) which was used to perform simulations within the isobaric, isothermal ensemble (NPT). The forces between ions were calculated in the same way as LD using the interatomic potentials, allowing the solution of Newton's Laws of Motion numerically over a finite time period for a simulation cell containing N ions. In the case of the {210} boundary the simulation cells contained 896 ions, 1440 for the {310} and {960} for the {410}. Periodic boundary conditions were applied to the cell to create an infinitely repeating system thus eliminating surface effects. Initial positions and velocities were assigned to each ion such that the ions start at their energy minimum positions with an velocity corresponding to the required temperature ensuring that the total momentum of the cell was zero. The positions of the ions at a given time step are calculated using a fifth order predictor-corrector method due to Gear (1971). The simulations were performed with the isothermal isobaric ensemble employing the Nosé-Hoover constant temperature method (Hoover 1985; Nosé 1984, 1990) which places the cell in contact with a heat bath allowing energy to transfer into or out of the cell, and the constant pressure method of Parrinello and Rahman (1981) that allows a dynamical change in both the lattice vectors and angles with time. Scaling runs of 5 ps were carried out to ensure that the cell has reached the correct pressure and temperature before data collection runs of 10 ps were carried out. The runs were extended by a further 10 ps if this was deemed necessary. For these calculations the MD calculations were used to examine structural transitions at the grain boundaries.

Results and discussions

Symmetric boundaries

Symmetric boundaries are so called because the lattice positions are mirrored about the grain boundary plane in the unrelaxed structure. The {210}, {310}, and {410} tilt grain boundaries are also described by the notation: $\Sigma = 5$, $\Sigma = 5$, and $\Sigma = 17$ where the angles between the boundaries are 53.1, 36.9, and 28.1 degrees, respectively. Our previous calculations (Harris et al. 1996) considered low pressures on the {210}, {310}, and {410} grain boundaries. In addition, zone center phonon calculations were performed for each pressure; an important result of this calculation was that an imaginary phonon frequency was calculated for the {210} boundary in the [001] direction at pressures above 17 GPa. This is caused by an instability in the vibrational mode and suggests that a structural transformation can occur to lower the free energy. Calculations on the {310} and {410} symmetric boundaries also showed the presence of imaginary modes at higher pressures, at 48 GPa for the {310} and 64 GPa for the {410} boundary. A plot of the phonon dispersion curve for the {310} boundary at 46 GPa, just before the mode becomes imaginary (Fig. 1) showed that a soft mode extends across the whole Brillouin zone perpendicular to the boundary plane in the [001] direction. This suggests the presence of a shear because the phase independence in this direction implies that the boundaries are moving independently. Animation of this imaginary mode for the {310} showed that the boundary sheared about the [001] axis as is illustrated for the {310} boundary in Figure 2 by showing the boundary and the extremes of the vibrational mode. A similar shear was calculated for the {210} and {410} boundaries and the result of increasing pressure before the onset of the shear is simply related to the increasing density of crosslinking interactions per unit area with increasing index.

To determine the structures formed by the boundaries

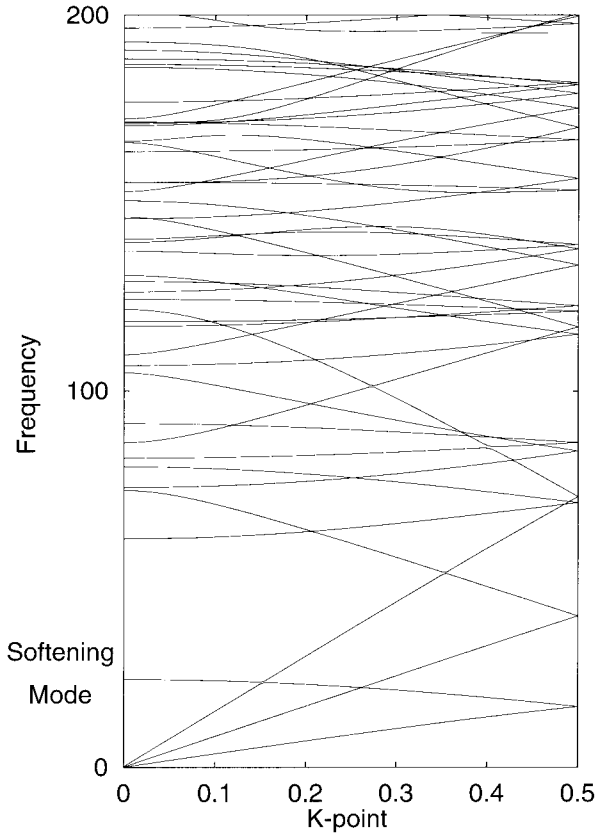

FIGURE 1. Phonon dispersion curve for the {310} tilt grain boundary in the [001] direction showing the softening phonon mode.

shearing, MD simulations were performed on the {210}, {310}, and {410} symmetric tilt grain boundaries at the pressures where the imaginary modes were calculated to occur from LD. In each case the boundary sheared during the scaling run and formed a new structure. The new structures were run at ambient pressures. The {310} (Fig. 3) was very similar to the asymmetric boundary suggested for NiO, isostructural with MgO, by Harding et al. (1989). Although the structure of this boundary looks like a perfect mirror, we have termed it asymmetric so it is clear that we are describing the boundary first identified by Harding et al. (1989). Similar structures were calculated for the {210} and {410} boundaries with the transformation found to be irreversible on release of pressure.

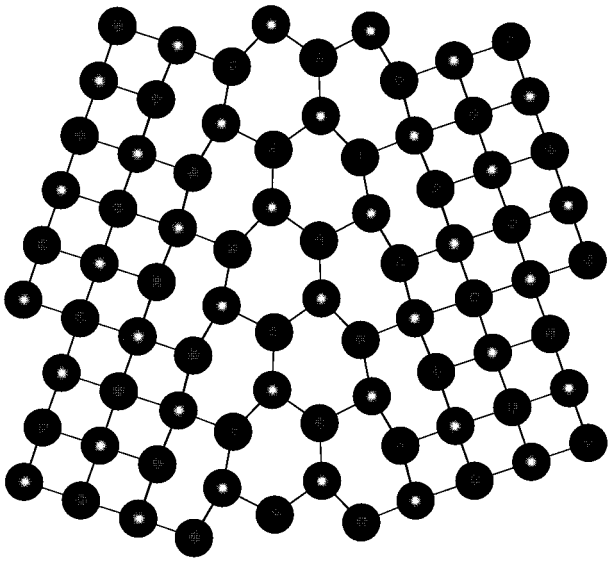

FIGURE 3. Minimized structures of the {310} asymmetric tilt grain boundary of MgO at 0 GPa and 600 K viewed down the [001] direction. Large circles = O atoms. Small circles = Mg atoms.

Asymmetric boundaries

Because the symmetric boundaries sheared to give asymmetric boundaries we modeled the {210}, {310}, and {410} asymmetric boundaries at pressures ranging from 0 GPa to 100 GPa at 600 K. The formation free energies, lattice energies, and *PV* terms are plotted for each of the grain boundaries in Figure 4. In each case the free energy increased with increasing pressure however

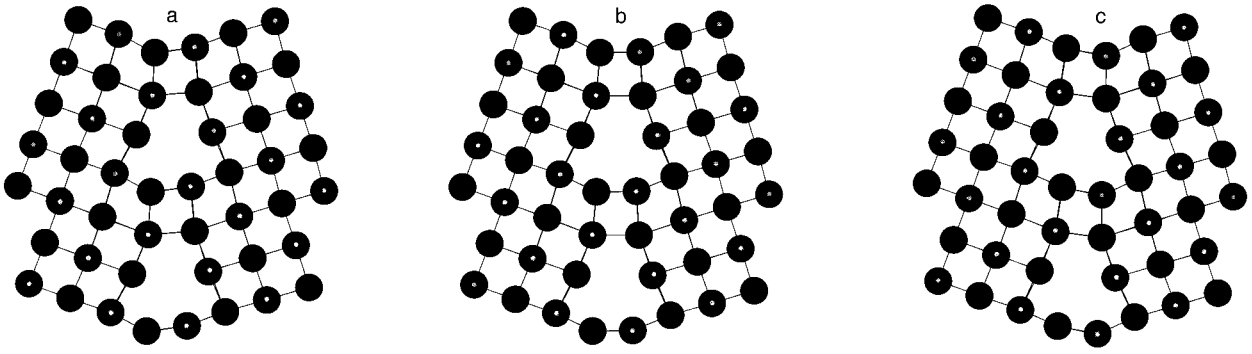

FIGURE 2. Snapshots of the imaginary mode in the {310} symmetric tilt grain boundary of MgO (**a**) distorted in one direction by the mode, (**b**) central position, and (**c**) distortion at the other extreme where the larger shaded circles are O atoms. Shows the shearing motion of the boundary.

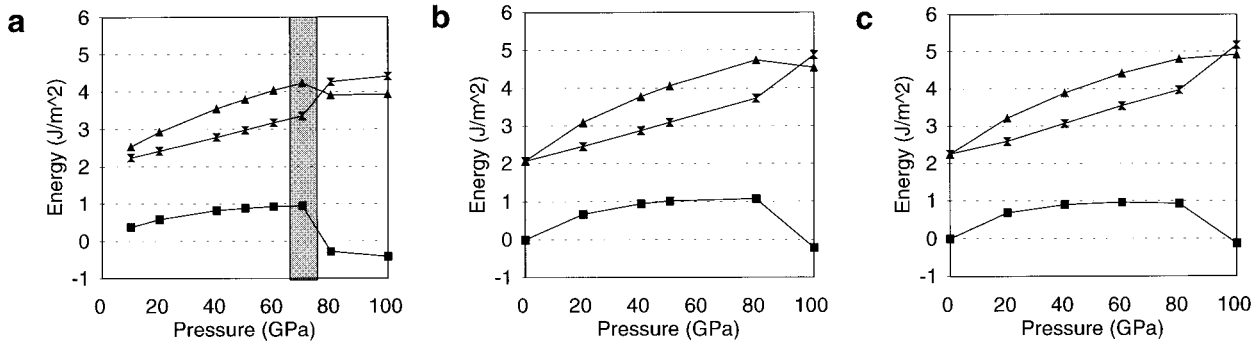

FIGURE 4. The energies of formation for (**a**) the (210), (**b**) the {310}, and (**c**) the {410} asymmetric tilt boundaries as a function of pressure at 600 K. Squares = *PV*; hourglasses = the static lattice energy; and triangles = the Gibbs Free energy. Shaded regions show where imaginary frequencies were calculated.

the rate of change of energy was lower than that found previously for the symmetric tilt boundaries. This was primarily due to the formation *PV* term, which for symmetric boundaries increased at a greater rate due to the larger dilation (the difference in volume between the grain boundary and the bulk per unit area of the boundary) resulting from the channels. As the pressure increased above 40 GPa, a reduction in the dilation due to compression of the free space at the boundaries (Fig. 3) caused the rate of change of the *PV* term for the asymmetric boundaries to decrease. The difference in the rate of change of free energy results in the asymmetric boundaries becoming more stable than the symmetric boundaries at high pressures. Comparison with the free energies of the symmetric boundaries showed that this occurred at approximately 10 to 20 GPa (Table 1). For example, the {310} symmetric boundary, which was 0.37 J/m^2 more stable than the asymmetric boundary at 0 GPa, was 0.42 J/m^2 less stable at 20 GPa.

In each of the three asymmetric boundaries studied there was a discontinuity in the lattice energy and *PV* term at 70, 80, and 82 GPa for the {210}, {310}, and {410}, respectively, leading to a reduction in the free energy. Examination of the phonon frequencies for each boundary revealed that as the pressure increased toward the point at which the discontinuity occurred one mode softened across the whole Brillouin zone, for example, the frequency in the {210} became imaginary at 70 GPa. In each case, after the discontinuity the phonon frequency increased again. The formation *PV* term for each boundary decreased sharply and became negative at approximately 100 GPa (Fig. 4) suggesting that the boundary was denser than the bulk. Examination of the 100 GPa structures revealed that a second shear had occurred, this time in the plane perpendicular to the boundary, leading to a very compact boundary that produced negative formation dilations. The structure {310} is shown in Figure 5.

The density of the boundary region can be seen to be close to that of the bulk with bonding along the full length of the boundaries and in an increased coordination of some of the boundary ions. For example, the {210} boundary at 100 GPa the structure contains sevenfold-coordinated magnesium and oxygen ions. The effect of

TABLE 1. Formation Gibbs free energies as a function of pressure

Pressure (GPa)	{210}		{310}		{410}	
	Sym	Asym	Sym	Asym	Sym	Asym
0	1.53	–	1.71	2.08	1.78	2.25
10	2.50	2.53	2.79	2.66	2.76	2.75
20	3.35	2.93	3.52	3.10	3.43	3.21
40	–	3.55	4.20	3.78	4.03	3.90
50	–	3.80	4.81	4.06	4.59	4.17
60	–	4.04	5.84	4.32	5.55	4.42
80	–	3.92	–	4.74	–	4.80
100	–	3.93	–	4.54	–	4.91

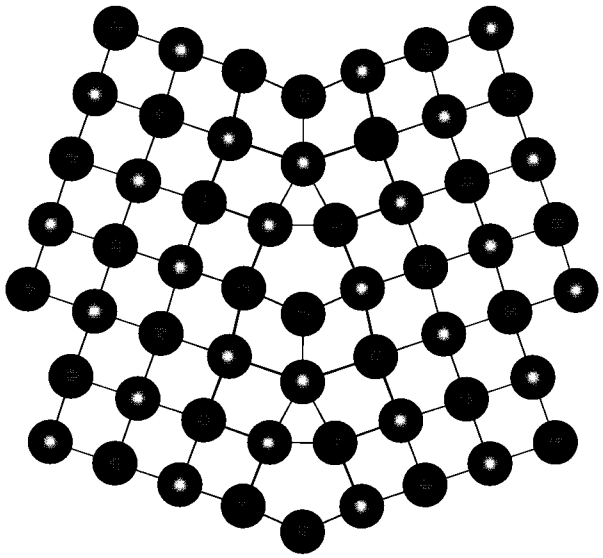

FIGURE 5. The minimized structures of the {310} asymmetric tilt grain boundary at 100 GPa and 600 K viewed down the [001] direction. Large circles = O atoms. Small circles = Mg atoms.

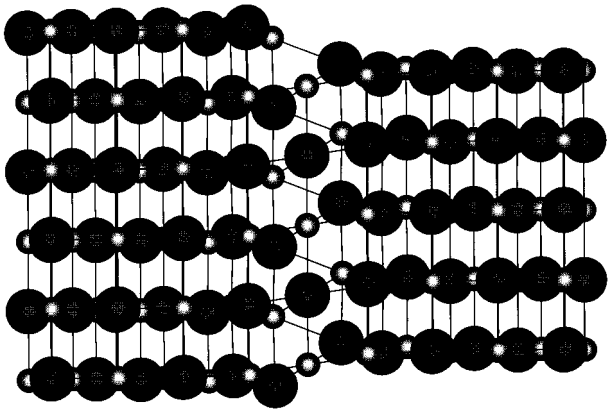

FIGURE 6. Side view of the minimized structure of the {310} asymmetric tilt grain boundary of MgO at 100 GPa and 600 K viewed down the grain boundary and showing the spiral dislocation structure along the [001] direction. Large circles = O atoms. Small circles = Mg atoms.

the shear is to generate a structure similar to a screw dislocation at the boundary. The planes of MgO are offset either side of the boundary and the triangular spiral of bonds running up through the center of the boundary in the [001] direction (Fig. 6). Similar structures were predicted for the other boundaries modeled.

The reversibility of these phase transitions was illustrated by using LD to reduce the pressure in stages back to 0 GPa. The Gibbs free energy, *PV* term, and lattice energy were plotted as a function of pressure in Figure 7. All data is given for completeness, although shaded regions on the graph are pressures where imaginary frequencies were found and thus the free energy cannot be defined properly. We have arbitrarily chosen to ignore imaginary frequencies from the calculation in these regions.

For both the {210} and {310} boundaries the structural transition was found to remain irreversible until pressures below the pressure at which the transition originally occurred. For example, the high pressure structure of the {210} boundary formed at approximately 80 GPa remained stable until the pressure was reduced to approximately 50 GPa. At this pressure the boundary reverted back to its original asymmetric structure as illustrated by the identical formation energies for structures before and after the transition had occurred at pressures below 50 GPa. Similarly, the high-pressure form of the {310} boundary remained stable until the pressure was below 80 GPa. However, the new structure was not dynamically stable and imaginary phonon frequencies were calculated for these boundaries. This suggests that the phase transition had not completely returned to the original structure upon the release of pressure to 10 GPa but instead formed a structure midway between the initial and high-pressure boundaries. The {410} boundary was found to be fully reversible upon release of pressure with the structure reverting back to the asymmetric boundary at the same pressure at which the original transformation was observed. However, on releasing the pressure to 0 GPa the structure was different from the initial 0 GPa structure and still retained an imaginary phonon frequency.

The observation of the asymmetric boundary is interesting when compared to previous studies on NiO. Duffy and Tasker (1983) and Harding et al. (1989) both predicted using atomistic simulation that the symmetric boundary was more stable that the asymmetric. In contrast, HREM experiments by Merkle and Smith (1987a, 1987b) and Merkle (1994) indicated that the structure was nearer to that predicted for the unstable asymmetric boundary (Harding 1989). Our simulations show that the asymmetric boundary becomes more stable at high pressure and that the transformation is not reversible on release of pressure, and may also help explain why this asymmetric structure is accessible to experiment. If the preparation conditions of the boundary (Merkle and Smith 1987b) were such that the required stresses were induced to allow the formation of the asymmetric boundary, the structure would then be locked in due to the irreversibility of the transformation.

ACKNOWLEDGMENTS

We thank the N.E.R.C. and E.P.S.R.C for financial support and M.S.I. for the use of their Insight II program for displaying the structures generated.

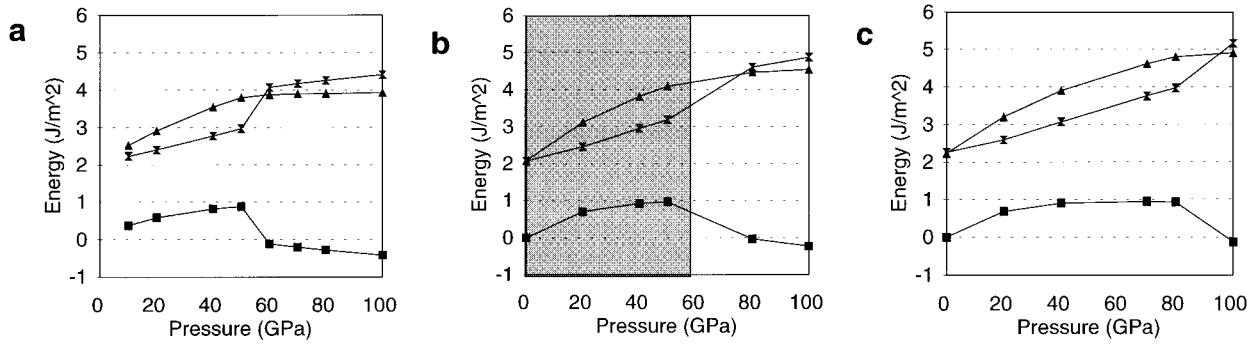

FIGURE 7. The energies of formation for (**a**) the (210), (**b**) the {310}, and (**c**) the {410} asymmetric tilt boundaries as a function of pressure at 600 K. United Kingdom Atomic Energy Authority.

References cited

Born, M. and Huang, K. (1954) Dynamic Theory of Crystal Lattice, Clarendon, Oxford.

Darco, P., Fava, F.F., Dovesi, R., and Saunders, V.R. (1996) Structural and electronic properties of pyrope garnet ($Mg_3Al_2Si_3O_{12}$). Journal of Physics: Condensed Matter, 8, 8815–8828.

Dick, B.G. and Overhauser, A.W. (1958) Theory of the dielectric constants of alkali halide crystals. Physical Review B, 112, 90–103.

Duffy, D.M. (1986) Grain boundaries in ionic crystals. Journal of Physics: Condensed Matter, 19, 4393–4412.

Duffy, D.M. and Tasker, P.W. (1983a) Computer simulation of {001} tilt grain boundaries in nickel oxide. Philosophical Magazine A—Defects and Mechanical Properties, 47, 817–825.

———(1983b) Computer simulation of {011} tilt grain boundaries in nickel oxide. Philosophical Magazine A—Defects and Mechanical Properties 48, 155–162.

Ewald, P.P. (1921) Annalen der Physik (Leipzig), 64, 253–287.

Gear, C.W. (1971) Numerical Initial Value Problems in Ordinary Differential Equations. Prentice Hall. Englewood Cliffs, New Jersey.

Harding, J.H., Parker, S.C., and Tasker, P.W. (1989) In J. Nowotny and W. Weppner, Eds., Non-Stoichiometric Compounds, Surfaces and Grain Boundaries and Structural Defects, UKEAE, Harwell.

Harris, D.J., Watson, G.W., and Parker, S.C. (1996) Atomistic simulation of the effect of temperature and pressure on the [001] symmetrical tilt grain boundaries of MgO. Philosophical Magazine A—Defects and Mechanical Properties, 74, 407–418.

Hoover, W.G. (1985) Canonical dynamics—equilibrium phase-space distributions. Physical Review A, 31, 1695–1697.

Katsura, T. (1997) Thermal diffusivity of periclase at high temperatures and high pressures. Physics of the Earth and Planetary Interiors, 191, 73–77.

Kingery, W.D. (1974) Plausible concepts necessary and sufficient for interpretation of ceramic grain boundary phenomena: I. grain boundary characteristics, structure, and electrostatic potential. Journal of the American Cerammic Society, 57, 1–8.

Matsui, M. (1989) Molecular dynamics study of the structural and thermodynamic properties of MgO crystal with quantum correction. Journal of Chemical Physics, 91, 489–494.

Matsui, M. and Price, G.D. (1992) Computer simulation of $MgSiO_3$ polymorphs. Physics and Chemistry of Minerals, 18, 365–372.

Merkle, K.L. (1994) Atomic structure of grain boundaries. Journal of Physics and Chemistry of Solids, 55, 991–1005.

Merkle, K.L. and Smith, D.J. (1987a) Atomic structure of symmetric tilt grain boundaries in NiO. Physical Review Letters, 59, 2887–2890.

———(1987b) Atomic resolution electron microscopy of NiO grain boundaries. Ultramicroscopy, 22, 57–70.

Nosé, S. (1984) A unified formulation of the constant temperature molecular dynamics methods. Journal of Chemical Physics, 81, 511–519.

———(1990) Constant temperature molecular dynamics. Journal of Physics: Condensed Matter, 2, SA115–SA119.

Parker, S.C. (1983) Prediction of mineral crystal structures. Solid State Ionics, 8, 179–186.

Parker, S.C. and Price, G.D. (1989) Computer modelling of phase transitions in minerals. Advances in Solid State Chemistry, 1, 295–327.

Parrinello, M. and Rahman, A. (1981) Polymorphic transitions in single crystals—a new molecular dynamics method. Journal of Applied Physics, 52, 7182–7190.

Poirier, J.P. (1985) Creep of Crystals, Cambridge University Press, Cambridge, U.K.

Sangster, M.J.L. and Stoneham, A.M. (1981) Calculations of off-centre displacements of divalent substitutional ions in CaO, SrO and BaO from model potentials. Philosophical Magazine B, 43, 597–608.

Sangster, M.J.L., Peckham, G., and Saunderson, D.H. (1970) Lattice dynamics of magnesium oxide. Journal of Physics: Condensed Matter, 3, 1026–1036.

Watson, G.W. and Parker, S.C. (1995) Dynamical instabilities in α-quartz and α-berlinite: a mechanism for amorphization. Physical Review B, 52, 13306–13309.

Watson, G.W., Wall, A., and Parker, S.C. (1994) A molecular dynamics simulation of the effect of high pressure on fast-ion conduction in a $MgSiO_3$-perovskite analogue; $KCaF_3$. Physics of the Earth and Planetary Interiors, 89, 137–144.

Watson, G.W., Tschaufesser, P., Wall, A., Jackson, R.A., and Parker, S.C. (1997) Lattice Energy and Free-energy Minimisation Techniques. In C.R.A. Catlow, Ed., Computer Modelling on Inorganic Crystallography, Academic Press, London.

Manuscript received December 29, 1997
Manuscript accepted August 22, 1998
Paper handled by Lars Stixrude